Magnetic Anisotropy in Ni-II-Y-III Binuclear Complexes: On the Importance of Both the First Coordination Sphere of the Ni-II Ion and the Y-III Ion Belonging to the Second Coordinat...

ARTICLE *in* INORGANIC CHEMISTRY · NOVEMBER 2011

Impact Factor: 4.76 · DOI: 10.1021/ic201623e · Source: PubMed

3 AUTHORS:

Rémi Maurice
Institut National de Physique Nucléaire et de...
27 PUBLICATIONS **355** CITATIONS
SEE PROFILE

Laure Vendier
Laboratoire de Chimie de Coordination.
176 PUBLICATIONS **2,711** CITATIONS
SEE PROFILE

Jean-Pierre Costes
French National Centre for Scientific Research
185 PUBLICATIONS **6,296** CITATIONS
SEE PROFILE

Inorganic Chemistry

ARTICLE

pubs.acs.org/IC

Magnetic Anisotropy in Ni^{II}—Y^{III} Binuclear Complexes: On the Importance of Both the First Coordination Sphere of the Ni^{II} Ion and the Y^{III} Ion Belonging to the Second Coordination Sphere

Rémi Maurice,[*,†,‡] Laure Vendier,[§,⊥] and Jean-Pierre Costes[*,§,⊥]

[†]Laboratoire de Chimie et de Physique Quantique, IRSAMC/UMR5626, Université de Toulouse III, 118 route de Narbonne, F-31062 Toulouse Cedex 4, France

[‡]Departament de Química Física i Inorganica, Universitat Rovira i Virgili, Marcel.lí Domingo s/n, 43007 Tarragona, Spain

[§]LCC (Laboratoire de Chimie de Coordination), CNRS, 205 route de Narbonne, F-31077 Toulouse, France

[⊥]UPS, INPT, LCC, Université de Toulouse, F-31077 Toulouse, France

Supporting Information

ABSTRACT: The synthesis of a new Ni^{II}—Y^{III} binuclear complex with a marked elongation axis in the first coordination sphere of the Ni^{II} ion is presented. Its zero-field splitting (ZFS) is studied by means of magnetic data and state-of-the-art ab initio calculations. A good agreement between the experimental and theoretical ZFS parameter values is encountered, validating the whole approach. The magnetic anisotropy axes are extracted from the ab initio calculations, showing that the elongation axis around the Ni^{II} ion corresponds to the hard axis of magnetization and that the sign of the axial *D* parameter is imposed by this axis. The Ni—Y axis is found to be an easy axis of magnetization, which is, however, not significant according to the sign of *D*. The already reported $[(H_2O)Ni(ovan)_2(\mu\text{-}NO_3)Y(ovan)(NO_3)]\cdot H_2O$ (ovan = *o*-vanillin) complex is then revisited. In this case, the elongation axis in the Ni^{II} coordination sphere is less marked and the ZFS is dominated by the effect of the Y^{III} ion belonging to the second coordination sphere. As a consequence, the *D* parameter is negative and the low-temperature behavior is dominated by the Ni—Y easy axis of magnetization. A competition between the first coordination sphere of the Ni^{II} ion and the electrostatic effect of the Y^{III} ion belonging to the second coordination sphere is then evidenced in both complexes, and the positive and negative *D* parameters are then linked to the relative importance of both effects in each complex.

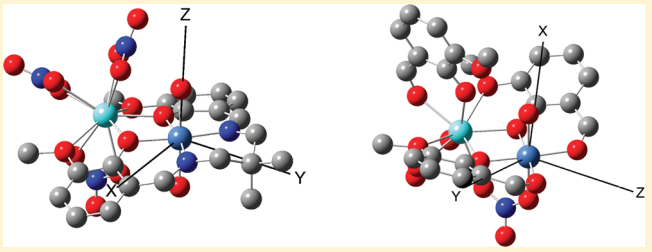

INTRODUCTION

Since the discovery of the peculiar magnetic properties of the so-called Mn_{12} compound,[1−3] the design of new transition-metal complexes with large magnetic anisotropy has become popular and several strategies have been followed. While in mononuclear complexes the anisotropy can be usually enlarged by maximizing the geometrical distortions of the first coordination sphere, in polynuclear complexes the anistropic intersite interactions are difficult to predict and hence the property of the whole system is far from being predictable.

Between mono- and binuclear complexes, a particular case of potential interest occurs when one of the two metal centers of a binuclear complex is diamagnetic, such as in Ni^{II}—Y^{III} complexes. In such cases, the zero-field splitting (ZFS) can be attributed only to the single-ion anisotropy of the Ni^{II} ion because the Y^{III} ion is a closed-shell system. Usually, the ZFS of Ni^{II} mononuclear complexes is interpreted only in terms of the crystal-field interaction brought by the first coordination sphere. Such works can be encountered, for instance, in the famous book of Abragam and Bleaney,[4] for which the axially distorted 6-coordinate Ni^{II} complexes are treated. Magneto-structural relations are then possible, and the sign of the *D* parameter can then be predicted only with geometrical considerations for homoleptic complexes, while the different donor characters of the ligands should be accounted for in the case of heteroleptic complexes.[5] However, if the Y^{III} ion is close enough to the Ni^{II} one, its presence in the second coordination sphere is susceptible to modifying in a nonnegligible way the ZFS of the magnetic ion. In this case, the influence of the second coordination sphere cannot be neglected and one has to go beyond simple crystal-field approaches that usually consider only the first coordination sphere of the magnetic ion.

In order to provide further insights into the anisotropy of such systems, state-of-the-art ab initio calculations will be used. The methodology is based on a two-step state-interaction (SI) approach. In a first step, the entire d^8 manifold is computed at

Received: July 28, 2011
Published: October 06, 2011

dx.doi.org/10.1021/ic201623e | *Inorg. Chem.* 2011, 50, 11075–11081

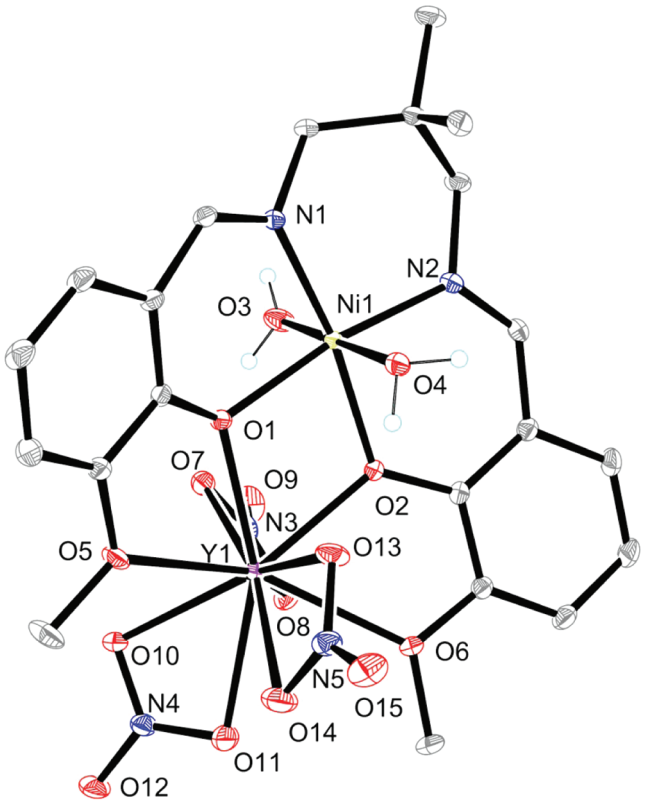

Figure 1. Plot of complex **1** with ellipsoids drawn at the 30% probability level and with partial atom numbering. H atoms, except those of the water molecules, have been omitted for clarity. Selected bond lengths [Å] and angles [deg]: Ni−O1 2.0351(9), Ni−O2 2.0327(9), Ni−N1 2.0060(11), Ni−N2 2.0196(10), Ni−O3 2.1358(9), Ni−O4 2.1514(9), Y−O1 2.3197(9), Y−O2 2.2827(8), Y−O5 2.5146(10), Y−O6 2.5157(9), Y−O7 2.4522(9), Y−O8 2.4697(10), Y−O10 2.4899(8), Y−O11 2.5159(11), Y−O13 2.4471(10), Y−O14 2.6033(11); O2−Y−O1 67.42(3), O1−Ni−O2 77.81(3), Ni−O1−Y 106.61(4), Ni−O2−Y 108.07(4).

the complete active space self-consistent-field (CASSCF) level, and the dynamic correlation can be accounted for by computing the correlated energies at the N-electron valence second-order perturbation theory (NEVPT2) level. A SI matrix including the effect of both the spin−orbit coupling (SOC) and the spin−spin coupling (SSC) is then diagonalized, and the ZFS parameters are extracted with the effective Hamiltonian theory. This general extraction process has been successfully applied in various mono- and binuclear complexes and allows one to extract both the anisotropic parameters and the magnetic anisotropy axes.[6−11]

Two complexes are considered in this work, namely, the $[(H_2O)_2Ni(L)Y(NO_3)_3]$ [**1**; L = *N*,*N*′-2,2-dimethylpropylenebis(3-methoxysalicylideneiminato) ligand] one (see Figure 1) and the already reported $[(H_2O)Ni(ovan)_2(\mu\text{-}NO_3)Y(ovan)(NO_3)]\cdot H_2O$ (ovan = *o*-vanillin) (**2**) one (see Figure 2).[12] After the synthesis and structure of **1** are reported, the magnetic data will be used in order to extract the ZFS parameters in both complexes. Then ab initio calculations that reproduce well the experimental data will be presented, and both the ZFS parameters and the magnetic anisotropy axes will be extracted, and the origin of the different *D* signs in **1** and **2** will be commented on.

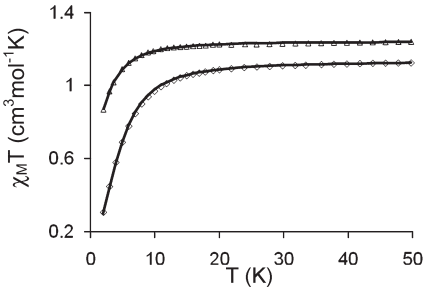

Figure 2. Temperature dependence of the $\chi_M T$ products for **1** (diamonds) and **2** (triangles) from 50 to 2 K. The solid lines correspond to the best data fits (D_{Ni} = 10.4 cm^{-1} and g = 2.12 for **1** and D_{Ni} = −6.6 cm^{-1} and g = 2.23 for **2**).

EXPERIMENTAL SECTION

$[LNi]\cdot 1.75H_2O$[13] [L = *N*,*N*′-2,2-dimethylpropylenebis(3-methoxysalicylideneiminato) ligand] and $[(H_2O)Ni(ovan)_2(\mu\text{-}NO_3)Y(ovan)(NO_3)]\cdot H_2O$[12] (**2**; ovan = deprotonated form of *o*-vanillin) were prepared as previously described. The metal salt $Y(NO_3)_3\cdot 6H_2O$ was used as purchased. High-grade acetone (Normapur, VWR) was used for the preparation of the complexes.

$[(H_2O)_2NiLY(NO_3)_3]$ (1). The addition of $Y(NO_3)_3\cdot 6H_2O$ (0.20 g, 0.52 mmol) to a stirred suspension of $[LNi]\cdot 1.75H_2O$ (0.2 g, 0.5 mmol) in acetone (10 mL) induced dissolution of the nickel complex with a color change. The mixture was stirred at room temperature, and the solution was reduced to half-volume. Slow evaporation yielded crystals suitable for X-ray analysis. Yield: 0.15 g (41%). Anal. Calcd for $C_{21}H_{28}N_5NiO_{15}Y$ (738.1): C, 34.2; H, 3.8; N, 9.5. Found: C, 33.9; H, 3.6; N, 9.1. IR: 3569 m, 3220 l, 1629 s, 1607 m, 1462 s, 1431 m, 1401 m, 1361 m, 1293 s, 1224 s, 1166 w, 1066 m, 1038 w, 960 w, 926 w, 853 w, 824 w, 781 w, 739 m, 645 w, 621 w cm^{-1}.

Physical Measurements. Elemental analyses were carried out at the Laboratoire de Chimie de Coordination Microanalytical Laboratory in Toulouse, France, for C, H, and N. IR spectra were recorded on a Perkin-Elmer Spectrum 100 FT-IR spectrophotometer using the attenuated total reflectance mode. Magnetic data were obtained with a Quantum Design MPMS SQUID susceptometer. Magnetic susceptibility measurements were performed in the 2−300 K temperature range in a 0.1 T applied magnetic field, and diamagnetic corrections were applied by using Pascal's constants.[14] Isothermal magnetization measurements were performed up to 5 T at 2 K. The magnetic susceptibilities have been computed by exact calculations of the energy levels associated with the spin Hamiltonian through diagonalization of the full matrix with a general program for axial and rhombic symmetries[15] and the magnetizations with the *MAGPACK* program package.[16] Least-squares fittings were accomplished with an adapted version of the function-minimization program *MINUIT*.[17]

Crystallographic Data Collection and Structure Determination for 1. Crystals of **1** were kept in the mother liquor until they were dipped into oil. The chosen crystals were mounted on a Mitegen micromount and quickly cooled to 180 K. The selected crystal of **1** (light purple, 0.15 × 0.12 × 0.05 mm^3) was mounted on a Bruker Kappa APEX II diffractometer using graphite-monochromated Mo Kα radiation (λ = 0.71073 Å) and equipped with an Oxford Cryosystems Cryostream Cooler Device. Data were collected at low temperature (180 K). The final unit-cell parameters have been obtained by means of least-squares refinements. The structures have been solved by direct methods using *SIR92*[18] and refined by means of least-squares procedures on F^2 with the program *SHELXL97*[19] included in the software package *WinGX*, version 1.63.[20] Positional parameters of the H atoms of water molecules in **1** were obtained from difference Fourier syntheses and

dx.doi.org/10.1021/ic201623e |*Inorg. Chem.* 2011, 50, 11075–11081

verified by the geometric parameters of the corresponding hydrogen bonds. The atomic scattering factors were taken from *International Tables for X-ray Crystallography*.[21] All non-H atoms were anisotropically refined, and in the last cycles of refinement, a weighting scheme was used, where weights are calculated from the following formula: $w = 1/[\sigma^2(F_o^2) + (aP)^2 + bP]$, where $P = (F_o^2 + 2F_c^2)/3$. Drawings of the molecules are performed with the program *ORTEP32* with 30% probability displacement ellipsoids for non-H atoms.[22]

COMPUTATIONAL SECTION

Several methodologies have been proposed and implemented over the last decades in order to compute the ZFS parameters. Among these, one may quote some density functional theory (DFT) based approaches, such as the pioneering one of Pederson and Khanna,[23] the hybrid ligand-field DFT approach of Atanasov et al.,[24,25] the spin DFT perturbation theory method of Aquino and Rodriguez,[26] and the perturbative and linear response theory based approaches of Neese.[27,28]

Alternatively, wave-function theory (WFT) based methods that allow one to handle the multideterminantal character of the spin eigenfunctions have been proposed. Usually, these methods use a two-step approximation. In the first step, a set of spin−orbit free states is computed at the CASSCF level, and the SOC and/or SSC is then introduced a posteriori as a perturbation of the spin-independent interactions. The inclusion of the SOC and/or SSC can be either based on quasi-degenerate perturbation theory,[29] as implemented, for instance, in the *ORCA* program,[30] or based on diagonalization of a SI matrix, as in the RASSI-SO scheme[31] implemented in *MOLCAS*.[32]

Although DFT-based methods have been successfully applied on various polynuclear complexes with nice agreement with experimental data,[33−38] WFT methods are usually more accurate that the DFT ones for mononuclear complexes.[27,39] Because this work focuses on Ni^{II}−Y^{III} complexes, which can be seen as particular Ni^{II} mononuclear complexes, a two-step WFT approach is chosen to provide accurate results, as in many reported works dealing with mono- and binuclear complexes[6−11,40−42] or mononuclear units of polynuclear complexes.[43−46] In order to include more effects than sum-over-states approaches, a SI method is used; i.e., a SI matrix is diagonalized in the second step of the calculation.

All calculations are performed with the *ORCA* program.[30] In the first step, the state-averaged CASSCF (SA-CASSCF) method is used to compute the spin−orbit free states belonging to the whole d^8 manifold (i.e., 10 triplet and 15 singlet spin−orbit free states). The scalar relativistic effects are neglected in the computation of the spin−orbit free states. The dynamic correlation is accounted for at second order of perturbation at the NEVPT2 level. The diagonal elements of the SI matrix may be replaced by the NEVPT2-correlated energies in order to take into account most of the dynamic correlation effects, while off-diagonal elements are computed by using the CASSCF wave functions. Both the SOC and SSC are included in the SI calculation. A mean-field SOC Hamiltonian[47,48] and the Breit−Pauli SSC Hamiltonian are used. The ZFS parameters D and E (axial and rhombic, respectively) and the magnetic axes frame are extracted with the effective Hamiltonian theory.[6]

The Def2 basis sets and the corresponding auxiliary basis sets[49] are used for all atoms with the following contraction schemes: Ni(5s3p2d1f), Y(6s4p3d1f), O(3s2p1d), N(3s2p1d), C(3s2p1d), and H(2s). Calculations performed on complex **1** showed that the use of larger basis sets does not affect the computed values in a significant way, such as in other transition-metal complexes,[11] validating the choice of these contraction schemes.

Because the computed property is strongly dependent on the geometry and because the experimental structures are usually more accurate than the optimized ones, leading to more accurate ZFS parameter values,[50] no geometrical optimizations have been performed. Complexes **1** and **2** are then taken in their experimental structure.

Table 1. Crystallographic Data for Complex 1

formula	$C_{21}H_{28}N_5NiO_{15}Y$
fw	738.10
space group	$P2_1$
a, Å	8.8100(7)
b, Å	15.9810(8)
c, Å	10.1120(6)
β, deg	91.449(4)
V, $Å^{-3}$	1423.24(16)
Z	2
ρ_{calcd}, g cm^{-3}	1.722
λ, Å	0.710 73
T, K	180(2)
μ(Mo Kα), mm^{-1}	2.770
R^a obs, all	0.0273, 0.0452
Rw^b obs, all	0.0430, 0.0457

[a] $R = \Sigma||F_o| - |F_c||/\Sigma|F_o|$. [b] $wR_2 = [\Sigma w(|F_o^2| - |F_c^2|)^2/\Sigma w|F_o^2|^2]^{1/2}$.

RESULTS AND DISCUSSION

Structural Analysis. The crystallographic data of complex **1** are collated in Table 1. The structural determination of the Ni−Y complex **1** (Figure 1) confirms that we have isolated a dinuclear Ni−Y entity in which the Ni ion occupies the inner N_2O_2 coordination site and the Y ion the outer O_2O_2 coordination site of the compartmental ligand. The two metal ions are bridged by the two deprotonated phenoxo O atoms, and the four Ni−O_2−Y atoms are almost coplanar, with the dihedral angle between the Ni−O1−O2 and Y−O1−O2 planes being equal to 2.72(5)°. The central core of the molecule is characterized by very similar Ni−O(i) (i = 1, 2) bond lengths [2.0351(9) and 2.0327(9) Å], slightly different Y−O(i) bonds [2.3197(9) and 2.2827(8) Å], and Ni−O(i)−Y angles of 106.61(4) and 108.07(4)°, giving a Ni−Y distance of 3.4959(3) Å. The Ni ion is in an octahedral environment, with the N_2O_2 atoms of the ligand defining the equatorial plane and two O atoms of water molecules occupying the apical positions with larger Ni−O bonds [2.1358(9) and 2.1514(9) Å]. These water molecules are involved in hydrogen bonds. So, a water molecule H_2O4 makes an intramolecular hydrogen bond O4−H40A···O13 with the coordinated nitrato O atom O13 and an intermolecular hydrogen bond O4−H40B···O10 with the coordinated nitrato O atom O10 of a neighboring molecule, thus giving a 1D chain in which the metal ions are separated by 8.810(1) Å. The second water molecule is also involved in an intramolecular hydrogen bond O3−H3A···O7 with the coordinated nitrato O atom O7 and in an intermolecular hydrogen bond O3−H3B···O15 with the noncoordinated nitrato O atom O15 of a neighboring molecule. These hydrogen bonds yield a final 2D plane, with a 10.112(1) Å separation of the metal ions in the second dimension. Eventually, these large intermolecular distances allow one to consider the only magnetic active Ni ions as well isolated from each other. The Y ion is 10-coordinate, with four O atoms coming from the ligand and six from the three chelating nitrato ions. The practically planar Y−O_2−Ni core induces a deformation of the molecule in a nonsymmetric boat conformation, with the phenyl cycles making dihedral angles of 12.7(1) and 23.2(1)° with the N_2O_2 equatorial

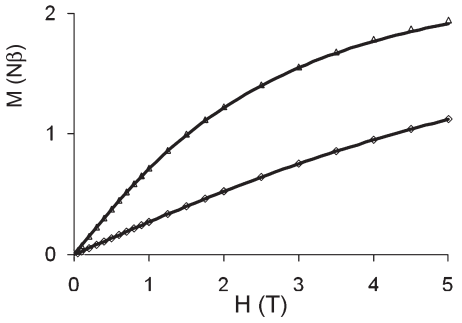

Figure 3. Field dependence of magnetization for **1** (diamonds) and **2** (triangles) at 2 K. The solid lines correspond to $D_{Ni} = 10.4\ cm^{-1}$, $E_{Ni} = 0.3\ cm^{-1}$, and $g = 2.12$ for **1** and to $D_{Ni} = -5.8\ cm^{-1}$ and $g = 2.23$ for **2**.

plane. Although this molecule has no chiral center, this peculiar conformation must be responsible for its crystallization in the noncentrosymmetric $P2_1$ space group.

The structural determination of complex **2** (Figure S1 in the Supporting Information) was previously described,[12] so that we only will recall the main differences between the two complexes. In the equatorial plane of the Ni ion, two N atoms are replaced by two O atoms for the metal center surrounded by two deprotonated *o*-vanillin ligands in place of the Schiff base ligand present in complex **1**. There is only a water molecule in the apical position and a nitrato ligand bridging the Ni and Y ions in the axial position. As a consequence, the Y ion is 9-coordinate, with four O atoms coming from the two ovan ligands, one from the bridging nitrato ligand, two from the chelating nitrato ligand, and the last two from a supplementary ovan ligand replacing the third nitrato ligand. If the equatorial Ni−O bond lengths, which vary from 1.9919(13) to 2.0210(14) Å, are quite similar to the ones present in complex **1**, the axial Ni−O bonds are shorter and equal to 2.0433(15) Å for O5 of the water ligand and to 2.0838(14) Å for Ni−O6 involving the bridging nitrato ligand. The central $Y-O_2-Ni$ core can be considered as planar, with a dihedral angle of 0.8(1)°, but the Ni−O(*i*)−Y angles (*i* = 3,4) are less important, 101.76(5) and 101.53(5)°, respectively, which induces a shorter Ni···Y distance [3.3244(3) Å]. The shorter intermolecular Ni···Ni distances are equal to 9.862(3) Å, so that the Ni ions can be again considered as well isolated from each other.

Magnetic Properties. *a. Experimental Studies.* According to the structural studies, the Ni ions are the only magnetic active metal centers in the two complexes **1** and **2** and are well isolated from each other. The magnetic susceptibilities of the two Ni−Y complexes have been measured in the 2−300 K temperature range under an applied magnetic field of 0.1 T. Thermal variation of the $\chi_M T$ product for complex **1** is displayed in Figure S2 in the Supporting Information (300−2 K) and in Figure 2 (50−2 K, diamonds), with χ_M being the molar magnetic susceptibility of the dinuclear species corrected for the diamagnetism of the ligands. $\chi_M T$, equal to 1.17 $cm^3\ mol^{-1}$ K at 300 K, remains practically constant until 30 K (1.10 $cm^3\ mol^{-1}$ K) before following an abrupt decrease to 0.30 $cm^3\ mol^{-1}$ K at 2 K. The room temperature $\chi_M T$ value does correspond to what is expected for an isolated Ni ion with a *g* parameter slightly larger than 2. The magnetic susceptibility has been computed by the exact calculation of the energy levels through diagonalization of the full energy matrix with a Hamiltonian introducing an axial ZFS term for Ni, $H = D_{Ni}S_z^2$. The best fit (solid line, Figures 2 and S2 in the Supporting Information) yields the following data: $D_{Ni} = 10.4\ cm^{-1}$, $g = 2.12$ with an *R* factor equal to 2.0×10^{-5}, $R = \Sigma[(\chi_M T)^{obs} - (\chi_M T)^{calc}]^2/\Sigma(\chi_M T)^{obs}]^2$. In order to check the validity of these results, the *MAGPACK* program has been used to fit the experimental magnetization curve at low temperature. The best simulation reported in Figure 3 (diamonds) needs introduction of a low rhombic *E* value ($E_{Ni} = 0.3\ cm^{-1}$).

Table 2. ZFS Parameters (in cm^{-1}) of 1 and 2 Extracted from a SI Calculation for Which the Diagonal Elements of the SI Matrix Can Be Either the CASSCF or the NEVPT2 Energies: Results Are Compared with Experiment

	1		2	
method	$D\ (cm^{-1})$	$E\ (cm^{-1})$	$D\ (cm^{-1})$	$E\ (cm^{-1})$
CASSCF	+15.4	2.2	−7.1	1.6
NEVPT2	+12.0	1.8	−5.3	1.2
Exp: $\chi T = f(T)$	+10.4	0.0	−6.6	0.0
Exp: $M = f(H)$	+10.4	0.3	−5.8	0.0

A similar behavior was observed for complex **2** (Figure S3 in the Supporting Information and Figure 2, triangles), with a constant $\chi_M T$ value from 300 K (1.23 $cm^3\ mol^{-1}$ K) to 11 K (1.20 $cm^3\ mol^{-1}$ K), followed by a decrease to 0.87 $cm^3\ mol^{-1}$ K at 2 K. A comparison of the $\chi_M T$ decrease at low temperature clearly indicates that the $\chi_M T$ decrease is lower in complex **2** than in complex **1**. The difference in the $\chi_M T$ decrease of the two complexes **1** and **2** and in the bond lengths of the respective Ni coordination spheres convinced us to reconsider the magnetic study of complex **2**. The best fit (solid lines, Figures 2 and S3 in the Supporting Information) gives $D_{Ni} = -6.6\ cm^{-1}$, $g = 2.23$, and $R = 2.0 \times 10^{-5}$. *MAGPACK* simulation of magnetization at 2 K with the above parameters confirms that a D_{Ni} value of $-5.8\ cm^{-1}$ appears to be more appropriate (Figure 3).

b. Ab Initio Calculations. In order to provide further insights into the ZFS parameters, ab initio calculations are performed. First, the computed and experimental ZFS parameters are compared for both complexes to validate the theoretical approach (see Table 2). At the CASSCF and NEVPT2 levels, the experimental *D* parameter is well reproduced in both complexes. Replacement of the diagonal elements of the SI matrix by the correlated NEVPT2 ones hardly affects the ZFS parameters in complexes **1** and **2**; hence, the dynamic correlation only plays a small role in the ZFS parameter in these complexes, as was already observed in 6-coordinate Ni^{II} mononuclear complexes.[6]

As is often observed,[6] the computed *E* parameters are much larger than the experimental ones obtained by magnetic measurements. This effect could be explained by either or both of the theoretical and experimental uncertainties. Further experiments would be necessary in order to validate or improve the experimental values, which is out of the scope of the present work. We conclude at this stage that the computed ZFS parameters are in good agreement with the experimental ones, particularly for the axial parameter, the main subject of the present work. As a consequence, the different *D* signs observed in **1** and **2** are confirmed.

Having validated the methodology of the calculation, the next step consists of determining the magnetic anisotropy axes. These axes are determined by extracting the entire second-rank ZFS tensor in an arbitrary axes frame, diagonalizing it to find its principal axes, and applying the standard conventions in molecular

dx.doi.org/10.1021/ic201623e |*Inorg. Chem.* 2011, 50, 11075–11081

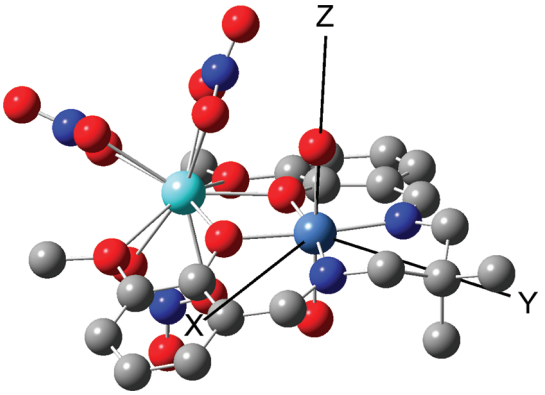

Figure 4. Ball-and-stick representation of **1**. The H atoms are omitted for clarity. The computed magnetic anisotropy axes *X*, *Y*, and *Z* are represented and labeled according to the standard conventions in molecular magnetism (see the text).

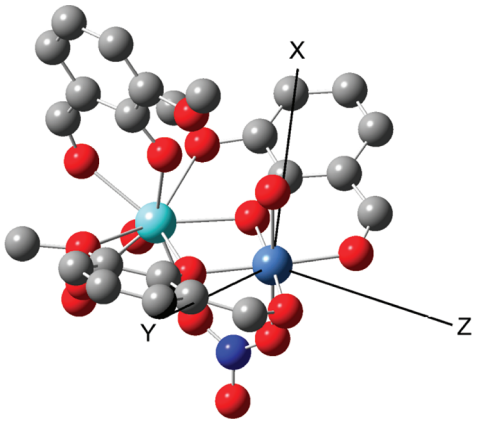

Figure 5. Ball-and-stick representation of **2**. The H atoms are omitted for clarity. The computed magnetic anisotropy axes *X*, *Y*, and *Z* are represented and labeled according to the standard conventions in molecular magnetism (see the text).

magnetism:

$$|D| = \left| D_{ZZ} - \frac{1}{2}(D_{XX} + D_{YY}) \right| > 3E \quad (1)$$

and

$$E = \frac{1}{2}(D_{XX} - D_{YY}) > 0 \quad (2)$$

The first convention ensures that the *Z* axis is univocally defined as the most different one of the three principal axes, while the second one allows one to label *X* and *Y* in a unique way. Hence, the magnetic anisotropy axes are univocally defined and labeled whatever the complex is. The magnetic anisotropy axes obtained at the NEVPT2 levels for **1** and **2** are presented in Figures 4 and 5, respectively.

In complex **1**, the *Z* axis is found in the elongation axis around the Ni^{II} ion, while the Ni−Y direction corresponds to the magnetic *Y* axis. In complex **2**, the elongation axis is the *X* magnetic axis, while the Ni−Y orientation is the *Z* axis. As a consequence, in both complexes, both the elongation axis and the Ni−Y orientations correspond to two of the three magnetic anisotropy axes. The roles of both the distortion of the first coordination sphere of the Ni^{II} ion and the presence of the Y^{III} ion in the second coordination sphere are then evidenced and deserve further discussion, which is the subject of the next paragraph.

c. Discussion. In order to further assess the respective roles of both the distortion of the first coordination sphere and the Y^{III} ion belonging to the second coordination sphere, the physical meaning of both the elongation axis and the Ni−Y direction have to be commented on.

The elongation axis in **1**, the *Z* magnetic axis, is a hard axis of magnetization that dominates the very low temperature behavior because the *D* parameter is positive. The role of the elongation axis can be understood with the rationalizing work of Abragam and Bleaney.[4] Indeed, they showed that axially elongated 6-coordinate Ni^{II} complexes lead to positive *D* values, with the elongation axis being then a hard axis of magnetization. This complex then follows these rules, showing that the first coordination sphere dominates here the ZFS.

In complex **2**, the *D* parameter is negative, showing that the ZFS is not dominated by the elongation of the first coordination sphere. One may remark that, in complex **2**, the elongation is much less important than in complex **1**, in agreement with the previous statements. The elongation axis, here labeled *X* according to the conventions used, represents a hard axis of magnetization, while the easy axis of magnetization *Z* is the most important anisotropy axis in the case of negative *D* values. As a consequence, in both complexes, the elongation axis plays the same role of a hard axis of magnetization. When this elongation axis is strongly marked, as in complex **1**, the ZFS is dominated by this effect and the *D* parameter is positive. In complex **2**, the ZFS is not dominated by the elongation, and the role of the Ni−Y direction has to be further analyzed.

In complex **1**, the Ni−Y orientation is an easy axis of magnetization due to its label *Y* obtained with the conventions of eqs 1 and 2, with the dominant effect coming actually from the hard axis of magnetization *Z* because *D* is positive. In complex **2**, which possesses a negative *D*, the Ni−Y direction is the *Z* anisotropy axis, i.e., the easy axis of magnetization; the ZFS is then dominated by the presence of the Y^{III} ion in the second coordination sphere, which imposes an easy axis of magnetization in this orientation. In both complexes, the roles of the first coordination sphere (i.e., elongation axis) and the Y^{III} ion are equivalent. The positive *D* in **1** is then explained by the dominant effect of the elongation because this elongation is well marked according to the geometrical structure, while in **2**, the Y^{III} ion of the second coordination sphere imposes a negative *D* value. The theoretical determination of the magnetic anisotropy axes was then crucial in order to explain the different *D* signs in the two presented cases.

In order to further assess the role of the Y^{III} ion, i.e., the reasons for which it imposes an easy axis of magnetization, the active orbitals are analyzed. The weight of the Y atomic orbitals is zero for all active orbitals. In other words, the d orbitals of the Ni^{II} ion do not overlap with the Y atomic orbitals, even if they do overlap with the bridging atoms between the Ni and Y atoms. As a consequence, the effect of the Y^{III} ion is mainly due to electrostatic effects and the large formal charge of this ion because the effect is already present at the CASSCF level in complex **2** and maintained when the dynamic correlation is accounted for (NEVPT2 level). The positive charge of the Y^{III} ion disturbs the crystal field felt by the Ni^{II} ion in such a way that the Ni−Y orientation becomes an easy axis of magnetization.

dx.doi.org/10.1021/ic201623e |*Inorg. Chem.* 2011, 50, 11075–11081

The large formal charge of the Y^{III} ion and the small Ni−Y distance are then responsible for the negative D value in **2**. One may remark that the Ni−Y distance is larger in **1**, inducing a smaller Y^{III} effect on the ZFS than that in **2**, which further differentiates the two complexes.

CONCLUSION

The ZFS of two $Ni^{II}-Y^{III}$ binuclear complexes has been studied by means of magnetic data and state-of-the-art ab initio calculations. A good agreement between the experimental and theoretical values allowed validation of the methodology of calculation. The determination of the magnetic anisotropy axes allowed rationalization of the ZFS of these $Ni^{II}-Y^{III}$ binuclear complexes by evidencing the role of the Y^{III} ion.

The different D signs in both complexes have been explained according to their molecular structure. It has been shown that a competition between the elongation of the first coordination sphere of the Ni^{II} ion and the presence of the Y^{III} ion in the second coordination sphere can result in a positive D if the elongation dominates or in a negative D if the electrostatic effect of the Y^{III} ion is the main effect.

While in both studied complexes the first and second coordination spheres showed antagonist effects, one important perspective consists of finding new structures for which the Y^{III} ion would enlarge the ZFS of the magnetic ion. Such a situation would occur when the first coordination sphere of the Ni^{II} ion would be tetragonally compressed. Then the effects of both the first and second coordination spheres would be synergistic, and a large negative D parameter might be expected. The ZFS of mononuclear units could then be tuned by adding some closed-shell ions with large formal charges in the second coordination sphere. Such original and new ways of tuning the anisotropy of transition-metal complexes might then provide new and interesting structures that would deserve further studies.

ASSOCIATED CONTENT

Supporting Information. Figures S1−S3 (plot of complex **2** and temperature dependence of the $\chi_M T$ products for **1** and **2** from 300 to 2 K) and crystallographic data of **1** in CIF format. This material is available free of charge via the Internet at http://pubs.acs.org.

AUTHOR INFORMATION

Corresponding Author

*E-mail: remi.maurice@gmail.com (R.M.), jean-pierre.costes@lcc-toulouse.fr (J.-P.C.).

ACKNOWLEDGMENT

This work was supported by the Spanish Ministry of Science and Innovation (Project CTQ2008-06644-C02-01), the Generalitat de Catalunya (Project 2009SGR462 and Xarxa d'R+D+I en Química Teòrica I Computacional, XRQTC), and the Agence National de la Recherche (ANR; Project TEMAMA ANR-09-BLAN-0195-01).

REFERENCES

(1) Caneschi, A.; Gatteschi, D.; Sessoli, R.; Barra, A. L.; Brunel, L. C.; Guillot, M. *J. Am. Chem. Soc.* **1991**, *113*, 5873–5874.
(2) Friedman, J.; Sarachik, M. P.; Tejada, J.; Ziolo, R. *Phys. Rev. Lett.* **1996**, *76*, 3830–3833.
(3) Thomas, L.; Lionti, F.; Ballou, R.; Gatteschi, D.; Sessoli, R.; Barbara, B. *Nature* **1996**, *383*, 145–147.
(4) Abragam, A.; Bleaney, B. *Electron Paramagnetic Resonance of Transition Ions*; Dover Publications: Dover, NY, 1986.
(5) Titiš, J.; Boča, R. *Inorg. Chem.* **2010**, *49*, 3971–3973.
(6) Maurice, R.; Bastardis, R.; de Graaf, C.; Suaud, N.; Mallah, T.; Guihéry, N. *J. Chem. Theory Comput.* **2009**, *5*, 2977–2984.
(7) Maurice, R.; de Graaf, C.; Guihéry, N. *J. Chem. Phys.* **2010**, *133*, 084307.
(8) Maurice, R.; Guihéry, N.; Bastardis, R.; de Graaf, C. *J. Chem. Theory Comput.* **2010**, *6*, 55–65.
(9) Maurice, R.; de Graaf, C.; Guihéry, N. *Phys. Rev. B* **2010**, *81*, 214427.
(10) Maurice, R.; Pradipto, A. M.; Guihéry, N.; Broer, R.; de Graaf, C. *J. Chem. Theory Comput.* **2010**, *6*, 3092–3101.
(11) Maurice, R.; Sivalingam, K.; Ganyushin, D.; Guihéry, N.; de Graaf, C.; Neese, F. *Inorg. Chem.* **2011**, *50*, 6229–6236.
(12) Costes, J.-P.; Vendier, L. *Eur. J. Inorg. Chem.* **2010**, 2768–2773.
(13) Costes, J. P.; Donnadieu, B.; Gheorghe, R.; Novitchi, G.; Tuchagues, J. P.; Vendier, L. *Eur. J. Inorg. Chem.* **2008**, 5235–5244.
(14) Pascal, P. *Ann. Chim. Phys.* **1910**, *19*, 5–70.
(15) Boudalis, A. K.; Clemente-Juan, J.-M.; Dahan, F.; Tuchagues, J.-P. *Inorg. Chem.* **2004**, *43*, 1574–1586.
(16) Borrás-Almenar, J. J.; Clemente-Juan, J. M.; Coronado, E.; Tsukerblat, B. S. *Inorg. Chem.* **1999**, *38*, 6081–6088. Borrás-Almenar, J. J.; Clemente-Juan, J. M.; Coronado, E.; Tsukerblat, B. S. *J. Comput. Chem.* **2001**, *22*, 985–991.
(17) James, F.; Roos, M. *Comput. Phys. Commun.* **1975**, *10*, 343–367.
(18) Altomare, A.; Cascarano, G.; Giacovazzo, C.; Guagliardi, A. *J. Appl. Crystallogr.* **1993**, *26*, 343–350.
(19) Sheldrick, G. M. *SHELX97 [Includes SHELXS97, SHELXL97, CIFTAB]—Programs for Crystal Structure Analysis*, release 97-2; Institüt für Anorganische Chemie der Universität: Göttingen, Germany, 1998.
(20) Farrugia, L. *J. Appl. Crystallogr.* **1999**, *32*, 837–838.
(21) *International Tables for X-ray Crystallography*; Kynoch Press: Birmingham, England, 1974; Vol. IV.
(22) Farrugia, L. *J. Appl. Crystallogr.* **1997**, *30*, 565–568.
(23) Pederson, M. R.; Khanna, S. N. *Phys. Rev. B* **1999**, *60*, 9566–9572.
(24) Atanasov, M.; Daul, C. A.; Rauzy, C. *Chem. Phys. Lett.* **2003**, *367*, 737–746.
(25) Borel, A.; Helm, L.; Daul, C. A. *Chem. Phys. Lett.* **2004**, *383*, 584–591.
(26) Aquino, F.; Rodriguez, J. H. *J. Chem. Phys.* **2005**, *123*, 204902.
(27) Neese, F. *J. Am. Chem. Soc.* **2006**, *128*, 10213–10222.
(28) Neese, F. *J. Chem. Phys.* **2007**, *127*, 164112.
(29) Ganyushin, D.; Neese, F. *J. Chem. Phys.* **2006**, *125*, 024103.
(30) Neese, F. *ORCA—An ab initio, density functional and semiempirical program package*, version 2.8; University of Bonn: Bonn, Germany.
(31) Malmqvist, P.-Å.; Roos, B. O.; Schimmelpfenning, B. *Chem. Phys. Lett.* **2002**, *357*, 230–240.
(32) Karlström, G.; Lindh, R.; Malmqvist, P.-Å.; Roos, B. O.; Ryde, U.; Veryazov, V.; Widmark, P.-O.; Cossi, M.; Schimmelpfenning, B.; Neogrady, P.; Seijo, L. *Comput. Mater. Sci.* **2003**, *28*, 222–239.
(33) Kortus, J.; Baruah, T.; Bernstein, N.; Pederson, M. R. *Phys. Rev. B* **2002**, *66*, 092403.
(34) Baruah, T.; Pederson, M. R. *Int. J. Quantum Chem.* **2003**, *93*, 324–331.
(35) Kortus, J.; Pederson, M. R.; Baruah, T.; Bernstein, N.; Hellberg, C. S. *Polyhedron* **2003**, *22*, 1871–1876.
(36) Park, K.; Pederson, M. R.; Richardson, S. L.; Aliagata-Alcalde, N.; Christou, G. *Phys. Rev. B* **2003**, *68*, 020405.
(37) Ribas-Ariño, J.; Baruah, T.; Pederson, M. R. *J. Chem. Phys.* **2005**, *123*, 044303.
(38) Ribas-Ariño, J.; Baruah, T.; Pederson, M. R. *J. Am. Chem. Soc.* **2006**, *128*, 9497–9505.

(39) Duboc, C.; Ganyushin, D.; Sivalingam, K.; Collomb, M.-N.; Neese, F. *J. Phys. Chem. A* **2010**, *114*, 10750–10758.
(40) de Graaf, C.; Sousa, C. *Int. J. Quantum Chem.* **2006**, *106*, 2470–2478.
(41) Cremades, E.; Ruiz, E. *Inorg. Chem.* **2011**, *50*, 4016–4020.
(42) Atanasov, M.; Ganyushin, D.; Pantazis, D. A.; Sivalingam, K.; Neese, F. *Inorg. Chem.* **2011**, *50*, 7460–7477.
(43) Petit, S.; Pilet, G.; Luneau, D.; Chibotaru, L.; Ungur, L. *Dalton Trans.* **2007**, 4582–4588.
(44) Chiboratu, L.; Ungur, L.; Aronica, C.; Elmoll, H.; Pilet, G.; Luneau, D. *J. Am. Chem. Soc.* **2008**, *130*, 12445–12455.
(45) Chibotaru, L.; Ungur, L.; Soncini, A. *Angew. Chem., Int. Ed.* **2008**, *47*, 4126–4129.
(46) Soncini, A.; Chibotaru, L. *Phys. Rev. B* **2008**, *77*, 220406.
(47) Neese, F. *J. Chem. Phys.* **2005**, *122*, 034107.
(48) Hess, B. A.; Marian, C. M.; Wahlgren, U.; Gropen, O. *Chem. Phys. Lett.* **1996**, *105*, 5321–5330.
(49) Weigend, F.; Ahlrichs, R. *Phys. Chem. Chem. Phys.* **2005**, *7*, 3297–3305.
(50) Zein, S.; Duboc, C.; Lubitz, W.; Neese, F. *Inorg. Chem.* **2008**, *47*, 134–142.